JET–P(98)08

β Scaling of Confinement

J P Christiansen, J G Cordey.

JET Joint Undertaking, Abingdon, Oxfordshire, OX14 3EA,

Preprint of a paper to be submitted for publication in
Nuclear Fusion

March 1998

ABSTRACT

Empirical scaling laws [1-3] for the confinement time τ_E in Tokamaks depend on dimensionless global plasma parameters in a way which is difficult to associate with some general plasma physics model. It is shown that such dependencies can arise form artefacts in the database used to derive the scaling expression. The artefacts involve inner relationships, e.g. collinearities between variables. For the ITER L-mode and H-mode databases it is shown that subsets of the scaling expressions are approximately constant. An alternative description of L-mode, ELM-free, small ELM and giant ELM H-mode data is given. A simple electrostatic physics model (plateau scaling) in which confinement is degraded by non-collisional processes, can describe global confinement data for all four confinement regimes; this common scaling features a multiplier C which is assigned a different value for each regime. The complex physics associated with MHD instabilities (ELM's, sawteeth, outer modes) is hidden in the multiplier C and attempts are made to uncover such physics. In these attempts global confinement are made to scale with physics models, electrostatic, MHD etc. rather than physics variables.

1. INTRODUCTION

Empirical scaling laws for the confinement time τ_E in Tokamaks such as Goldston or Kaye-Goldston [1], ITER89P [2] and ITER93H [3] are based on multi-machine databases, i.e. databases containing data from several different sized Tokamaks. These multi-machine scaling laws like several earlier single machine scaling laws appear to be different; however by transformations of the scaling laws these can be unified into scaling expressions based on physics models [4]. The differences between the scaling laws can then be accounted for by different β-scalings: Table V of ref. [4] lists 16 scaling laws showing different β dependencies

$$\tau_E \sim \beta^x \qquad -1.5 < x < 1.5 \tag{1}$$

as apparently plausible scalings. This dichotomy is the central subject of the present paper which will examine experimental evidence for β-scaling from individual Tokamaks as well as data from the ITER L-mode and H-mode databases. Tokamak scaling laws have two principal purposes: extrapolations of τ_E can be made outside the τ_E range of the database; secondly a scaling law serves as an empirical benchmark for pulses on existing Tokamaks via the H_{89} or H_{93} factor where

$$H_{93H} = \tau_E \,/\, \tau_{93H} \tag{2}$$

H_{93H} measures how well in a single experiment the confinement time τ_E compares against the database as a whole represented by the scaling.

We use the Connor-Taylor representation [5] which links τ_E to a global average diffusivity $\langle\chi\rangle$

$$\tau_E = \frac{3}{4}\,\frac{a^2}{<\chi>} = \frac{3}{4}\frac{a^2}{\chi_B F} = \tau_B / F(...) \qquad (3)$$

The Bohm diffusivity is $\chi_B = <T>/B$. The dimensionless function F [3, 4, 5] is characterised by its dependence upon a set of dimensionless parameters which characterise the plasma configuration globally. Which set of parameters that enter F as arguments is a matter of choice as it depends on which transport physics model applies: the review by Connor [5] presents a variety of expressions for F; ref. [6] lists a possible set of up to 18 dimensionless plasma parameters. In general Eq. (3) is an implicit equation for τ_E which appears on both the LHS and RHS.

The H_{93H} factor is a consequence of a linear regression on data for a set of nine variables (confinement time τ_E, radius a, density n, current I_ϕ, power P, aspect ratio ε, elongation κ, ion mass M, field B_ϕ). The selected data is the ELM free data in the ITER H-mode database DB2 [3] and the result can be written in the form

$$F_{93H} = C_{93H}\, \rho_*^{0.78}\, \nu_*^{0.28}\, \beta^{1.24}\, \varepsilon^{5.05}\, \kappa^{-0.15}\, M^{-1.23}\, q^{-1.03} \qquad (4)$$

C_{93H} is a multiplier and the parameters in (4) represent global averages of local plasma parameters [3, 4, 5, 6]. A recent update to (4) derived from the database DB3 [7] has produced F_{97H} which is similar to F_{93H} given by (4), but the number C_{97H} differs from C_{93H} as do the exponents for normalised Larmor radius ρ_*, collisionality ν_*, poloidal β, inverse aspect ratio ε, elongation κ, ion mass M cylindrical safety factor q. The empirical result (4) cannot easily be associated with some physics model, e.g. ideal-resistive MHD, ion temperature gradient driven turbulence, resistive fluid turbulence, collisional drift waves etc., for the following reasons

i) as $\beta \to 0$ an electrostatic scaling expression should be recovered.

ii) the pronounced ε scaling should strongly favour Stellarators over Tokamaks.

iii) the M scaling is opposite to that associated with an ion gyro Bohm model.

In order to investigate the origin of the various scalings of eq. (4) we show in Fig. 1 the distribution function f (H_{93H}) for the ELM free DB2 data on which H_{93H} is based (curve marked with circles). As can be expected the half-width of f (H_{93H}) is of the order of the r.m.s. error σ in the fittings. Also shown in Fig. 1 is the distribution function f (H_{93H}) for the ELMy data (curved marked with crosses). The distribution of the ELMy data is similar to that of the ELM free data, but with a mean value of ~ 0.85; the representation $F_{ELMy} = 1.40\, F_{93H}$ is the one advanced by the ITER database

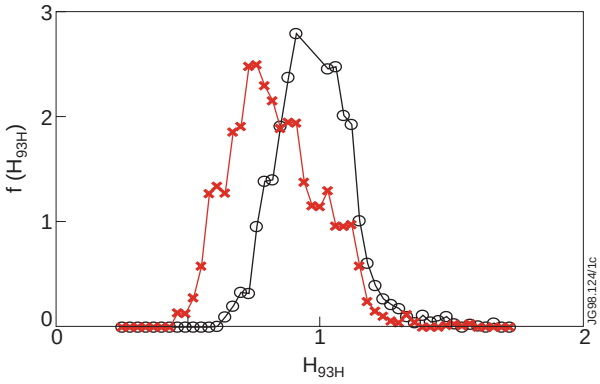

Fig.1: Distribution functions for H factors in database DB2. Circles refer to ELMfree data and crosses to ELMy data.

working group and determined on DIIID in [8] (notice that the number 1.40 in F_{ELMy} corresponds to a number 0.85 in τ_E because Eqs. (3, 4) involve implicit expressions for τ_E). The physics associated with the plasma energy losses arising from small or "grassy" to large or giant ELM's is complex; the representation of ELM types and how to quantify their effect on each Tokamak constitutes a problem which has been looked at by the ITER database expert group [3] since its inception; a "zero order solution" is thus the fixed reduction (factor 0.85) of τ_ε for all Tokamaks. Another problem is illustrated in Fig. 2. The DB2 ELM free data on the H_{93H} factor (Eq. 2) is shown against poloidal β as used in Eq. (4). While the data as a whole shows no trend w.r.t. β, the data for each Tokamak separately exhibits a definite proportionality; this trend is particularly pronounced for the JET and PDX data. The H_{93H} and β proportionality for a given Tokamak shown by the dashed lines in Figure 2 can be expressed as

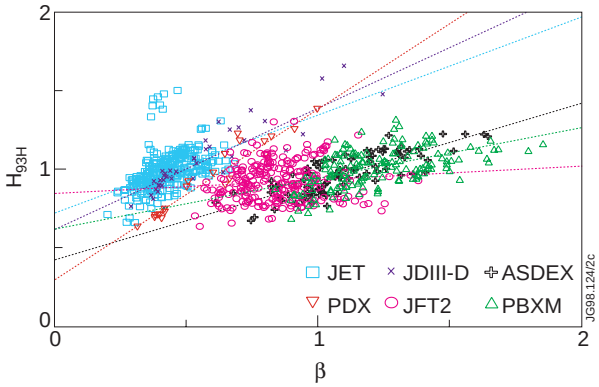

Fig.2: The H factor for each single Tokamak is proportional to β. DB2 ELMfree data.

$$H_{93H} \approx c\beta \quad \text{at fixed a and } \varepsilon \tag{5}$$

As much as H_{93H} is a "goodness" factor it also represents a range of uncertainty $0.5 < H_{93H} < 1.5$. Such a range can arise from i) core physics effects ii) spatial profile shapes, iii) edge pressure pedestal; none of these effects can be described by the present global data. The range of uncertainty is important for extrapolations made using Eq. (4). Extrapolation from the existing ITER databases to ITER has recently been discussed in [7, 9]; formally an extrapolation can be made in any direction of a multi-dimensional space; standard statistical procedures determine the uncertainty range $\Delta\tau_E$ associated with a prediction τ_{93H}. It is however well known that limitations on the data do not permit extrapolations to be made in certain directions i.e. those of the "least" principal components [2, 3, 7, 9]. To overcome such limitations one can adopt the similarity scaling approach [10]. The step in the confinement time τ_E for a specific operating regime of JET to the confinement time for a similar regime in DIIID or in ITER involve only a scaling w.r.t. normalised Larmor radius ρ_*. Similarity scaling experiments have been carried out for L-mode plasmas on DIIID [11], TFTR [6], JET [12] and for H-mode plasmas on DIIID [13] and JET [14]. These experiments have concentrated on the scaling of F with ρ_* but attempts have also been made to determine F (ν_*), F (β) and recently F(q) [15].

One would hope, possibly expect, that similarity experiments will supplement, as well as confirm empirical scaling laws. Results from ρ_* and ν_*, β scans on JET [14] are presented in section 2. While the ρ_* and ν_* scans agree with ITER93H, the β scans do not; this last result is consistent with the JET β dependence. The discrepancy is examined in section 3 in an analysis

of the ITER L-mode and H-mode data bases. The results of the analysis show how data artefacts (inner relations and collinearities) can influence the scaling expression for the confinement time τ_E.

Section 4 describes the consequences of removing the database artefacts: a simple confinement scaling emerges from both the L-mode, ELM free and ELMy H-mode data. This common scaling corresponds to some simple electrostatic physics model (like plateau scaling) in which confinement is degraded by non-collisional processes. The scaling features one multiplier C_{gB} rather than the eight variables of Eq. (4). The four values of C_{gB} required to describe L-mode, ELM free, small ELM, giant ELM data indicates that C_{gB} contains hidden physics. Section 5 outlines our attempts to unravel such physics employing complex non-linear confinement models. The results of Sections 4 and 5 offer a common physics description of the data rather than a set of 4 empirical scaling laws. This is discussed in Section 6.

2. SIMILARITY SCALING EXPERIMENTS ON JET

Over a period of three years 120 pulses on JET have formed a part of experimental campaigns aimed at establishing "ITER similarity pulses", H-mode power threshold scans; scans of ρ_*, ν_* and β. All pulses are NBI heated steady ELMy H-modes with mostly type I ELM's (grassy ELM's). The plasma geometry is fixed and resembles both that planned for ITER as well as the geometry used on DIIID [9] for ITER support studies. The data from this set of pulses have variations in F arising from variations of just one variable, either ρ_*, ν_* or β. The data set also includes 4 "identity" pulses in which attempts have been made to match the values of the 7 arguments of F on JET to the values for pulses on DIIID and C-MOD, i.e. $F = F_o$ for inter-machine comparisons. A preliminary analysis of the data has been presented in [14].

An analysis of the global parameters τ_E, τ_B, ρ_* etc. has been made in which the total energy W_{dia} measured by the diamagnetic loop has been corrected for the fast ion energy content W_f. A fit to data from calculations with the TRANSP code yields the approximate formulae

$$W_f = 7.5\ 10^{14}\ P_{NBI} < T_e > / < n_e > \qquad (6)$$

where P_{NBI} is the net injected beam power and the angular brackets refer to volume averages. The results from this analysis are most easily presented graphically. We show in Fig. 3 the H_{93H} versus β for the entire set of 120 pulses. Fig. 3 encapsulates the problem addressed in this paper just as Fig. 2 did. For $\beta < 1$ there is an apparent linear relationship between H_{93H} and β as expressed by Eq. (5). Unlike the ITER ELM free H-mode data shown in Fig. 2 and which exhibits variations in ε, κ, M, q, the JET data represented by Fig. 3 has been selected for the following ITER-JET similarities

$$\varepsilon = 0.34, \quad \kappa = 1.7, \quad M = 2, \quad q_{95} = 3.2$$

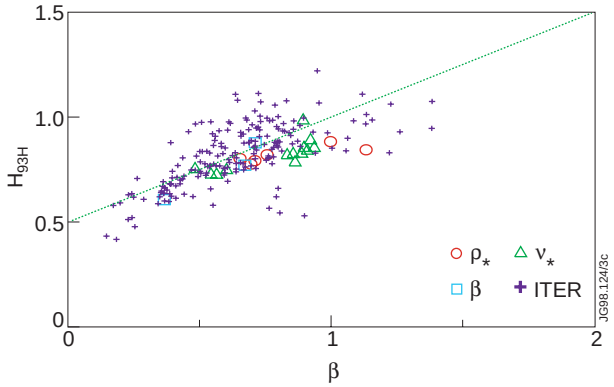

Fig.3: The dotted line indicates hoe the H factor is proportional to β. JET ELMy H-mode data from ITER similarity scans.

A linear regression on this JET data set can thus be made only in the variables ρ_*, ν_*, β; the result demonstrates that $F \sim \beta^{\circ}$.

For the similarity studies we have selected pairs of pulses which are matched as well as possible with respect to constant values of (ν_*, β), (ρ_*, β), (ρ_*, ν_*) for the scans of respectively ρ_*, ν_*, β. These selected pairs of pulses are marked with a circle, triangle, square for the scans of ρ_*, ν_*, β respectively in Figure 3. In Figures 4a, 4c and 4e we indicate how well these pulses are matched. For each scan we show in Figs. 4b, 4d and 4f the resulting responses in F against the variations in respectively ρ_*, ν_*, β. Fig. 4b demonstrates the experimental difficulty of varying ρ_* by more than a factor 2, but the response in F for 3 of 4 pulses is in agreement with the $F \sim \rho_*$ or gyro Bohm variation of ITER93H (Eq. 4); this result has also been obtained on DIIID [13]; In Fig. 1d we note that ν_* has been varied by a factor 80 and the inferred scaling $F \sim \nu_*^{0.3}$ also agrees with Eq. (4); however Fig. 4f demonstrates that the variation in β by factors 1.6 and 2 produces only a weak response in F in contrast to the predictions of ITER93H; the residual β scaling in H_{93H} demonstrated by Fig. 3 for the selected β scan (marked by squares in figure 3) cancels the predicted scaling in Eq. (4). In other words the similarity pulses are "as similar as possible except for their H_{93H} values".SKuch a discrepancy prompts an examination into the source of the pronounced β scaling in equ.. (4).

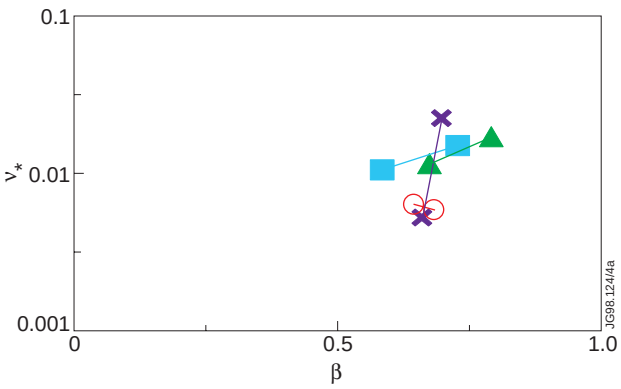

Fig.4a: ρ_*scan, four pairs of pulses with matching values of ν_* and β.

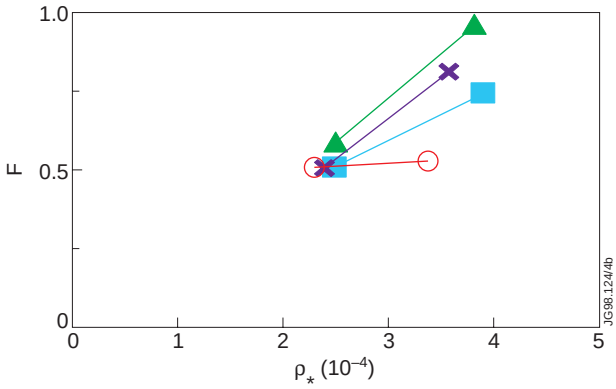

Fig.4b: ρ_*scan shows $F \sim \rho_*$ like ITER93H.

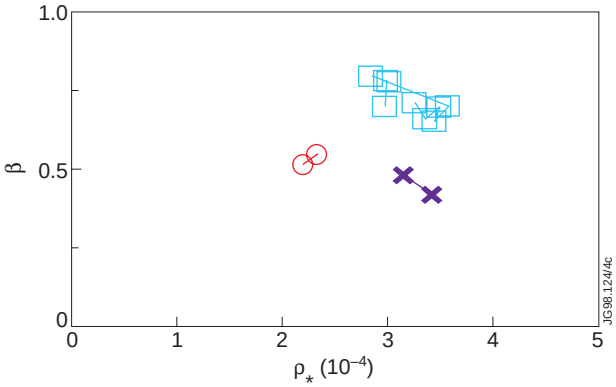

Fig.4c: ν_* scan has 13 well matched pulses.

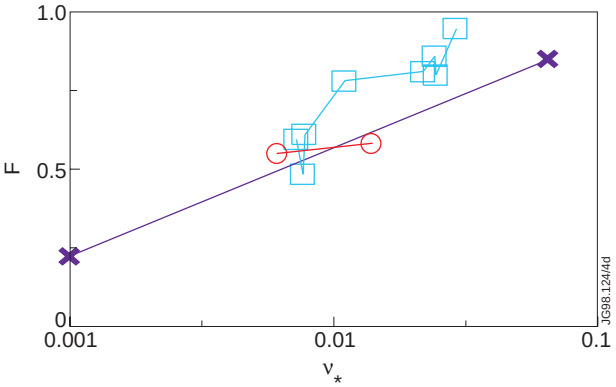

Fig.4d: ν_* scan shows $F \sim \nu_*^{1/3}$ like ITER93H..

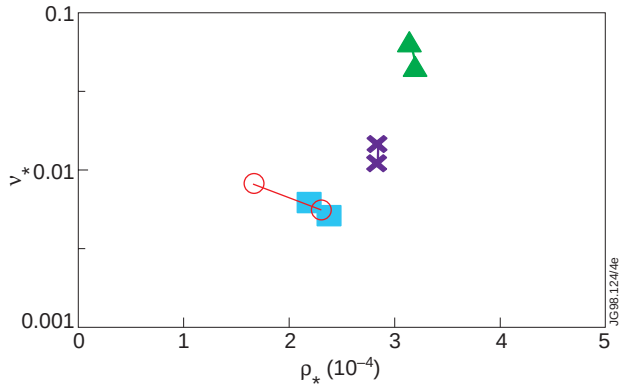

Fig.4e: β scan has pulses well matched.

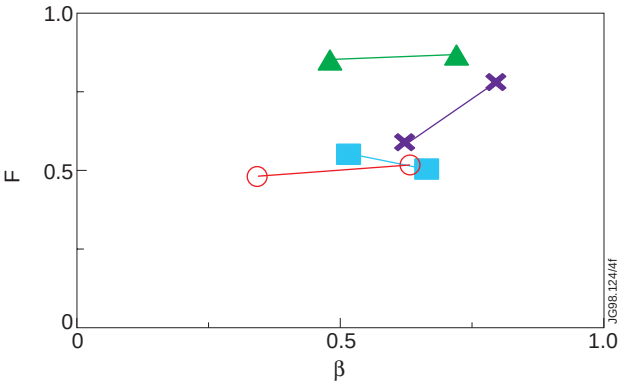

Fig.4f: β dependence unlike ITER93H.

3. β, ε, M, κ, q SCALING OF ITER93H

The linear regression techniques which have been applied to the ITER L and H-mode data [1-3] are standard text book techniques. The regression analyses assign a cause-effect status to each of the eight independent variables of Eqs. (3-4) with respect to the dependent variable τ_E. The resulting scaling of τ_ε with one independent variable depends not only on the data properties in the data base of that variable, but it also depends on the data properties of the entire set of independent variables: the data correlation matrices which determine a scaling exponent x_j and its statistical exponent δx_j for a variable j involve inner products of dependent and independent variables. The stability of a result x, against changes to the data in the database can be tested by excluding or adding data, e.g. via the jack-knifing technique [16] or via comparing results from the new DB3 database [7] with those of the previous DB2 database [3]. Such tests have been carried out by the ITER expert database group and we quote as an example the β scaling of the ELM free H-mode data in DB2 and in DB3 (see Eq. 4):

$$x_\beta \text{ (DB2)} = 1.24, \quad x_\beta \text{ (DB3)} = 0.79, \quad \delta x_\beta = 0.05 \qquad (7)$$

Thus we learn that the change Δx_β exceeds the statistical uncertainty δy_β by a factor 10. Such a result has prompted us to investigate which data correlations contribute most to a given

result such as x_β. The investigations have involved a lengthy series of calculations on the two data correlations matrices

$$S_{ij} = \sum_k y_{ik}\, y_{jk}, \quad C_{j\tau} = \sum_k y_{ik} \log \tau_{Ek}, \quad x_i = \left(S_{ij}\right)^{-1} C_{j\tau} \tag{8}$$

where y_{ik} is e.g. $\log \rho_{*\kappa}$ and κ is the observation index scanning the data base.

There is no separate method available for deciding if the confinement time τ_E does indeed scale with any or all of the eight dependent variables of Eqs. (3-4. The assumption made is that the regression (8) will describe the extent of the scaling, e.g. $x_i \approx 0.01$ or $x_i \approx 1$, and that the result justifies the assumption via the data correlation. To verify this assertion we have carried out calculations like (8) in which subsets of the eight dependent variables are selected. The technical details will not be given in this paper but we illustrate our findings by the following point: The scaling of τ_E with β, i.e. x_β, always has $x_\beta < 0$ unless the assumption $\tau_E \sim \varepsilon^{x_\varepsilon}$ is made; if this assumption is made then x_β changes to + 1.24. The data correlation between ε and β in the database DB2 is shown in Fig. 5 (ELM free data); it is the dominant contribution to x_β given by (8). There is thus an inner relationship or collinearisity between the independent and dependent variable ($\beta \sim \tau_E$) in the data base.

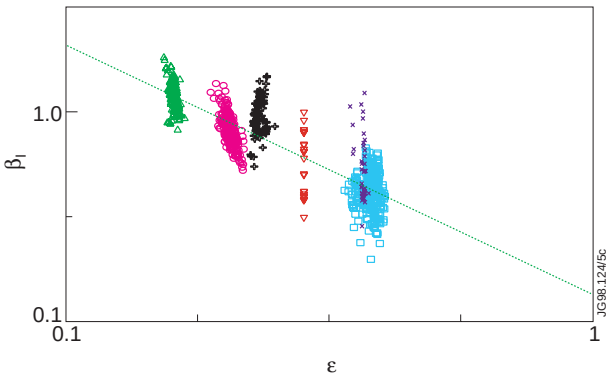

Fig.5: There is a strong correlation between ε and β_l in the DB2 ELMfree data. Symbol legend as in Figure 2.

The results of our investigation can be summarised by the following artefact in the DB2 database

$$h_{93H} = \beta\, \varepsilon^{5/3}\, \kappa^{1/9}\, M^{-1/3}\, q^{-2/3} \approx \text{ const.} \tag{9}$$

with an r.m.s. error of 18%. Fig. 6 shows the DB2 ELM free data on h_{93H} plotted against H_{93H}. The "constant" H_{93H} which describes pulse to pulse and Tokamak to Tokamak variations is as "constant" as the database artefact h_{93H}. The quasi-elliptic shape of the cloud of data points has its major axis aligned with the $h_{93H} = H_{93H}$ line; some unquantified part of the H_{93H} distribution function (Fig. 1) can therefore be explained by the data artefact h_{93H}. Also it can be shown that h_{93H} does not

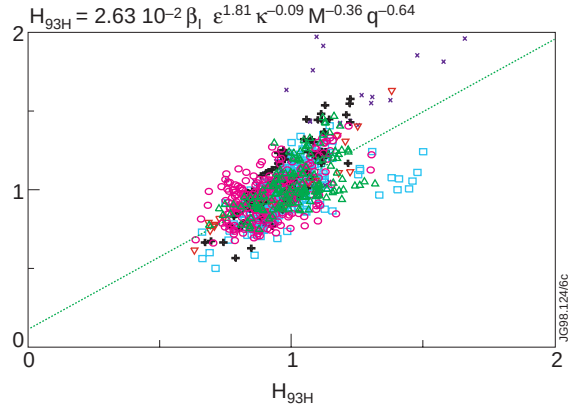

Fig.6: The database artefact h is as 'constant' as the H factor with a σ=18.0% in the DB2 ELMfree data. Symbol legend as in Figure 2.

by itself depend on F; thus h_{93H} does not contain substantial variations in confinement; the constancy of h_{93H} is a consequence of the DB2 data population in β, ε, κ, M, q space, i.e. a consequence of the operating regimes of the 6 Tokamaks contributing data to the ITER DB2 database.

4. ALTERNATIVE: ELIMINATION OF β

The data analysis procedures described in sections 1 and 3 have used the ITER H-mode DB2 ELM free data [3]. These procedures can be repeated for the ELM free, small ELM's, giant ELM's and the ITER L-mode data [2]; we reference these 4 databases by subscripts H, S, G, L, respectively; all H + L-mode data is subscripted HL. The result of the analysis is 5 scalings F_{97H}, F_{97S}, F_{97G}, F_{97L}, F_{97HL} for which the constants C_{97} and the exponents x_ρ, x_ν, of Eq. (4) are listed in Table I together with the r.m.s. errors σ expressed in %. When the H, S, G, L data is merged into the HL-data it is necessary in a fit to this data to allow for four separate constants C_{97H}, C_{97S} etc. if the same exponents x_ρ, x_ν etc. are to apply to all the HL-data. The r.m.s. errors σ in the five "free" fits to F as given by Eq. (4) are all less than or of the order the inferred relative errors $\Delta\tau_{Eth}/\tau_{Eth}$ on the confinement time. Thus only statistical arguments, not physics arguments, would favour the four individual scalings over the fifth and common scaling. We notice from Table I that the changes Δx_ρ, Δx_β etc. to the exponents from one fit to another all exceed the statistical uncertainties δx (row 6) by a large margin. It seems likely, although no proof can be given, that the differences between these five scalings result not from different physics properties, but from the different properties of the data base population of β, ε, M, q space as explained in the previous section. A linear regression on the variables of Eq. (4) assigns the cause - effect status to such variables via data correlations. The changes to the scalings caused by changes to the data, i.e. the stability of the scaling do not appear to have a physics origin and we therefore look for an alternative representation of the confinement data.

Data	N	$C_{93}10^2$	x_ρ	x_ν	x_β	x_ε	x_κ	x_M	κ_q	σ(%)
ELM free	858	310^{10}	0.78	0.28	1.24	5.04	-0.15	-1.23	-1.02	12.2
small ELM	345	310^{-4}	1.11	0.08	1.19	6.40	-1.56	-1.19	-0.72	14.3
giant ELM	422	10^{-2}	1.12	0.05	0.63	4.47	-0.40	0.65	-0.99	13.5
L-mode	1295	99	-0.03	-0.19	1.42	4.26	-0.84	-0.7	-0.09	16.7
H + L mode	2920	0.03	0.04	1.35	4.51	-1.33	-1.07	-0.66	18.1	
δx	0.09	0.03	0.06	0.2	0.12	0.1	0.1			

Table I. The r.m.s. errors σ from free fits to the exponents x_ρ, x_ν etc. of Eq. (4) for each of the four confinement regimes separately and for all four regimes combined; the statistical uncertainties δx are given in the last row.

The constancy of h_H (or h_S, h_G, h_L) can eliminate some of the dependencies shown in Eq. (4) and in Table I. It does not however provide us with any proof of which variables in F to eliminate. A variety of new scalings can therefore be attempted. A measure, $\delta\sigma$, of the influence on the data fitting from a variable can be obtained by omitting such a variable and recording the change $\delta\sigma$ to the r.m.s. error σ; however we emphasise that such a measure is only for guidance. A simple set of calculation reveal that ε is by far the most "influential" variable while q, κ, ν_* are the least "influential" variables.

A straight forward substitution of h_H (Eq. 9) into F_{93H} (Eq. 4) eliminates β and leads to the following expression

$$F_H = F_{93H} / h_H = C_H \, \rho_*^{0.78} \, \varepsilon^{2.81} \quad \nu_*^{0.28} \left(\kappa^{0.04} \, M^{-0.78} \, q^{-0.23} \right) \tag{10}$$

The bracketed term contains the less "influential" variables. Expressions similar to (10) are obtained when h_S, h_G, h_L are inserted into the appropriate scalings for F. We examine for F_H, F_S, F_G, F_L, F_{LH} the results from fits to the form (10) without the bracketed term i.e.

$$F = C \, \rho_* \, \nu_*^{x_\nu} \, \varepsilon^{x_\varepsilon} \tag{11}$$

Table II presents the values of x_ν, x_ε, C as well as the r.m.s. error σ. The dependence of F upon ν_* for L-mode data is opposite to that of the H-mode data and opposite to a classical dependence; this difference is presently not understood. However the combined L and H-mode data shows no dependence upon ν_* ; that same tendency is evident from Table I.

Data	N	C 10^{-3}	x_ν	x_ε	σ(%)
ELM free	858	6.2	0.32	3.02	16.7
small ELM	345	3.1	0.34	3.24	17.3
giant ELM	422	8.9	0.17	2.87	15.0
L-mode	1295	8.5	-0.42	3.97	21.6
H + L mode	2920		0.03	3.03	23.7

Table II Results from a repeat of the exercises used for Table I but fitting to F of Eq. (11).

The alternative description of the combined ITER L-mode and H-mode data to the four scaling expressions F_{97H} etc. of Table I emerges from the fifth row of Table II. It corresponds to a very basic gyro Bohm model

$$F_{gB} = C \quad \rho_* \, \varepsilon^3 \tag{12}$$

This simple description includes four values for the constant C applying to the ELM free, small ELM, giant ELM and L-mode data. By omitting the dependences of τ_E upon ν_*, β, κ, H and q the r.m.s. error σ will of course increase as "five degrees of freedom" are dropped; the

increases $\Delta\sigma$ range from 1% to 5%. The standard plot of τ_E vs $\tau_{gB} = \tau_B/F_{gB}$ is shown in Figure 7 for all 2920 data points. The simple data description by Eq. (12) allows most τ_E data to lie within the error range, a range which the authors estimate to be 20-25%. Both L and H-mode feature the same basic gyro-Bohm physics; this contrasts with the difference between ITER89P (Bohm) and ITER93H (gyro-Bohm).

The scaling expression (12) strongly resembles the plateau scaling proposed by Lackner [17].

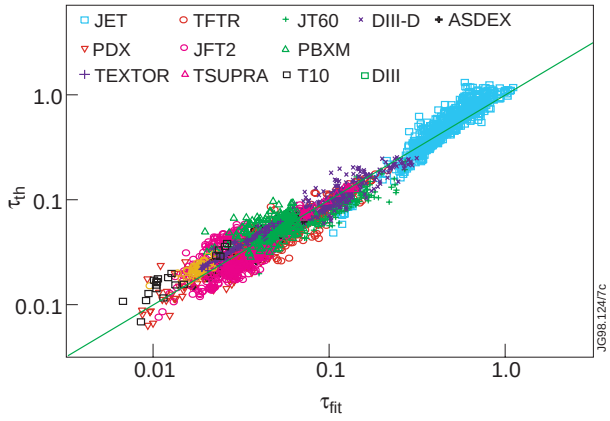

Fig.7: An alternative representation (Eq.12) of 2914 L & H-mode data with σ-23.6%.

5. HIDDEN PHYSICS

F_{gB} (Eq. 12) offers a very basic physics representation of global confinement data. It is however unlikely that the differences between L-mode and H-mode physics as well as effects from small and giant ELM's can be explained simply by assigning four different values to the constant C in Eq. (12). In this section we discuss some of the physics which may be hidden in C.

Each of the four confinement regimes is assumed to be governed by the same "core confinement physics model" given by Eq. (12). A transition from one regime to another is rapid as it usually involves an MHD instability: sawtooth instability, localised n = 1 or n = 2 instability, small ELM, giant ELM. The non-linear evolution of the MHD instability lasts many Alfvén transit times before the plasma is brought to the new regime; however compared to a confinement timescale (10 ms -1 sec range in the ITER L and H-mode databases) the transition times from one confinement regime to another is extremely short. One description such as the multi-mode model [18] represents a multi-regime physics by the sum

$$< \chi > \; = \; \sum_j C_j \, \chi_j \quad \text{or} \quad \tau_E^{-1} = \sum_j C_j \, \tau_j^{-1} \tag{13a}$$

In (13a) various physical loss processes due to η_i modes [19], resistive ballooning modes etc. are modelled by an expression χ_j which is weighted by the multiplier C_j. In another possible description the total stored plasma energy W is separated into parts which are identified with the four confinement regimes

$$W \; = \; \sum_j C_j \, W_j \quad \text{or} \quad \tau_E = \sum_j C_j \, \tau_j \tag{13b}$$

The energies W_j can include: the core confinement $P\tau_{gB}$ derived from Eq. (12); an edge pedestal energy formed at the L → H transition; the loss of energy released during giant ELM's; this amount can be up to 8% of W on JET; a complex time evolution is found to take place as evidenced by recent data from the JET soft x-ray diagnostic [20].

We have attempted to describe the four different regimes of confinement by a variety of combinations of scaling expressions. Eqs. (14) below define some of the scalings for τ_j which can be used in either (13a) or (13b):

$$\tau_{neo} = \tau_B \rho_*^{-1} \nu_*^{-1} \varepsilon^{3/2} q^{-2} \tag{14a}$$

$$\tau_{NN} = \tau_B \rho_*^{-1} \nu_*^{-1/3} \varepsilon^{3} \tag{14b}$$

$$\tau_{gB} = \tau_B \rho_*^{-1} \varepsilon^{3} \tag{14c}$$

$$\tau_{MHD} = \tau_B \rho_*^{-1} \beta^{1/2} \kappa^{1/2} \varepsilon \tag{14d}$$

$$\tau_{RFT} = \tau_B \rho_*^{-1} \nu_*^{-1} \beta^{1/2} \tag{14e}$$

$$\tau_{\beta} = \tau_B \beta_N^{-1} \tag{14f}$$

$$\tau_{thr} = \tau_B \rho_*^{-1} \nu_*^{-1} \beta^{3/4} \varepsilon^{1/2} \kappa^{1/4} q^{-1} \tag{14g}$$

Eq. (14a) is the neoclassical scaling; (14b) is the "near neoclassical" scaling in the first two rows of Table II while τ_{gB} corresponds to Eq. (12); τ_{MHD} is the ideal MHD scaling (Alfvén transit time) and τ_{RFT} corresponds to resistive fluid turbulence; τ_β is a representation of the pedestal effect in which the pedestal energy is governed by MHD stability; it is represented here as well as in [21] by the simple form of Eq. (14f); Eq. (14g) is the result of rewriting one of the ITER H-mode threshold scaling laws [22]. When some subset of Eqs. (14) is selected and inserted in (13a) or (13b) we arrive at a non-linear equation for τ_E of the general form

$$G = \left(\tau_E - \sum_j C_j \tau_j \right) / \tau_E = \sum_j G_j \tau_E^{x_j} \tag{15}$$

Minima of the dimensionless number G are sought w.r.t. variations of the constants C_j. The result from a lengthy series of calculations can be summarised as follows: no particular combination stands out as the most appropriate data description, say in terms of the statistical r.m.s. error. However, the research has demonstrated that the constant C of Eq. (12) does contain hidden physics. We can emphasise this point by selecting one particular combination of scalings (14b, d, e, f) for which Eq. (15) reduces to the following 2nd order equation in τ_E

$$G = \left(1 - G_{RFT}\right) \tau_E^2 + \left(G_{MHD} + G_\beta\right) \tau_E + G_{NN} \tag{16}$$

We apply this combination to ELM free, small ELM and giant ELM data each governed by a choice for the constants C_{NN}, C_{MHD}, C_{RFT} and C_β. The minimisation of G leads to the values of the constants shown in Table III. In this example there is a clear separation of small ELM and giant ELM data: Figures 8a, b show respectively H-mode data on $C_\beta \tau_\beta$ and on $C_{MHD} \tau_{MHD}$ plotted against τ_E. It is surprising that, by adding three physics scalings (16d, e, f) to the scaling given by (14b), there is hardly any change to r.m.s. error; this can be checked by comparing the first rows of Table II with those of Table III. The pedestal energy representing H-mode confinement is eroded by ideal MHD and - or resistive fluid turbulence effects since C_{MHD} and C_{RFT} are negative. We stress once again that the data description via Eqs. (13a, b) are complex and no clear choice has emerged.

Data	C_{NN} (10^{-5})	C_{MHD} (10^{6})	C_β	C_{RFT} (10^{-3})	σ(%)
ELM free	6.9	-2.0	0.46	-2.0	14.8
small ELM	4.0	-0.3	0.23	-0.01	16.6
giant ELM	2.6	0.0	0.32	-0.04	14.9
L-mode		0.5	0.1	-2.0	24.9

Table III Values of the constants for the scalings (14b, d, e, f) used in Eq. (13b) as a representation of H-mode data. The values for σ when compared with those of the four top rows in Table II, show no dramatic reductions.

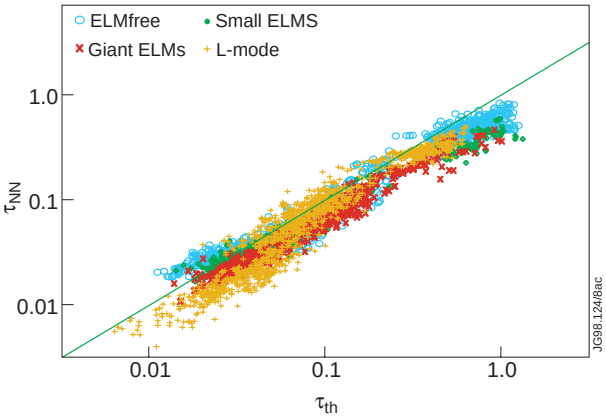

Fig.8a: In the data representation of a multi-mode model (Eq.16) the electrostatic τ_{NN} scaling (Eq.14b) is similar to that of τ_{th}.

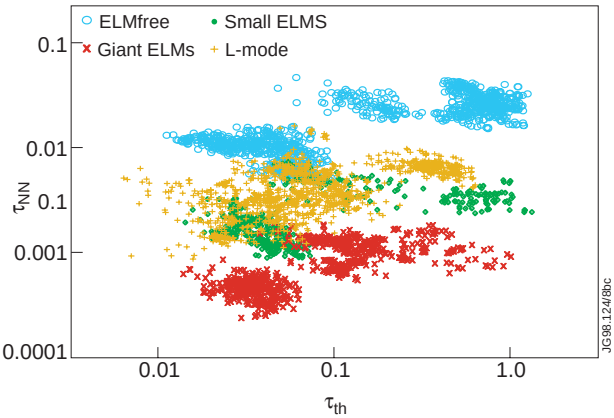

Fig.8b: The ideal MHD scaling (Eq.14d) separates the four confinement regimes.

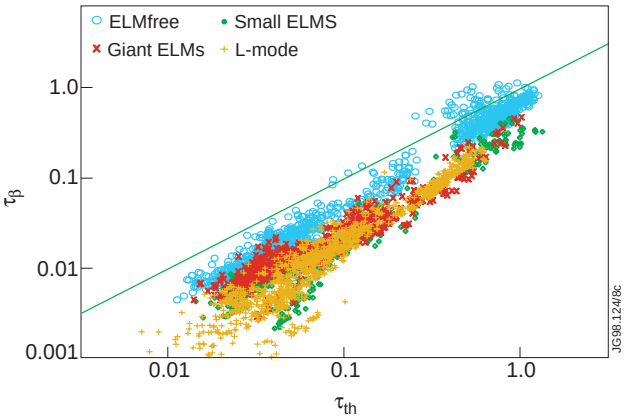

Fig.8c: The edge pedestal (Eq.14e) increases from L-mode to small to giant ELMs and is largest for ELMfree H-modes.

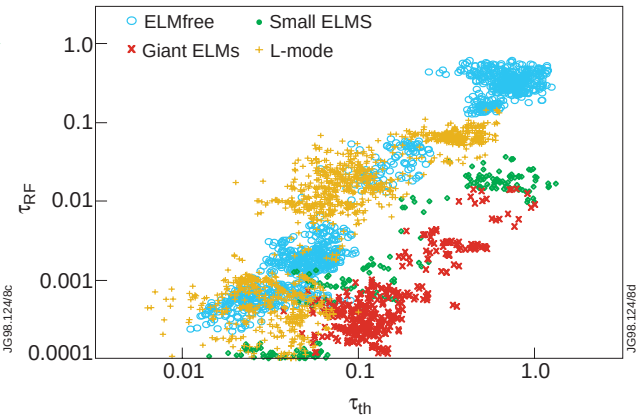

Fig.8d:The resistive fluid turbulence scaling (Eq.14f) of the multimode model of Eq.(16) differs in the four confinement regimes.

6. DISCUSSION

In its dimensionally correct form (Eq. 4) the ITER93H scaling expression features 7 exponents and 2 constants. The values of these are the result of a linear regression analysis which assigns a cause-effect status to each the variables in Eq. (4). Eq. (9) for h_{93H} applying to the ELM free data (similar expressions apply to h_{93E}, h_{93S}, h_{93L}) demonstrates how artefacts in the ITER database can produce confinement scalings which are not observed on individual Tokamaks. By substituting h_{93} into Eq. (4) we have eliminated most of the spurious dependencies in Eq. (4). The alternative description i.e. Eq. (12) is basic and simple. We have stressed that although this simple scaling gives a reasonable fit to the data it is insufficient to describe L-mode, small-giant ELM and ELM free data: the constant C of Eq. (13) contains hidden physics.

Our attempts to establish additional dependencies of global confinement data have lead to non-linear scaling expressions (13). From the numerous combinations of basic physics models (14) that have been tested against the L and H-mode data on global confinement we have been unable to select one single set of models as the best representation of the data. A particular choice (Eq. 16) of models reveals though how it is possible to separate ELM free, small ELM and giant ELM data. We conclude however that not only is further research required to make advances in the data description of global confinement data but the latter needs to be supplemented by additional parameters, e.g. via plasma edge measurements.

ACKNOWLEDGEMENT

This work is based on the ITER databases and the work of the ITER Expert Database Group is acknowledged. The careful reading of the manuscript by D. Ward is also acknowledged.

REFERENCES

[1] Goldston, R.J., Plasma Phys. Controll. Fusion 26 (1984) 87.
Kaye, S.M. Goldston, R.I., Nucl. Fusion 25 (1985) 65.
Kaye, S.M., Phys. Fluids 28 (1985) 2327.

[2] Yushmanov, P.N., Takizuka, T., Riedel, K.S., et al. Nucl. Fusion 30 (1990) 1999. Kaye, S.M., Barnes, C.W., Bell, M.G. Phys. Fluids B2 (1990) 2926. Kay, S.M. et al. Nucl. Fusion **37** (1997) 1303.

[3] ITER H-mode Database Working Group: Nucl. Fusion 32 (1992) 291.
Nucl. Fusion 34 (1994) 131.

[4] Christiansen, J.P., Cordey, J.G., Thomsen, K., Nucl. fusion 30 (1990) 1885.

[5] Connor, J.W., Taylor, J.B., Nucl. Fusion **17** (1977) 1047.
Connor, J.W., Plasma Physics Controll. Fusion 20 (1988) 619.

[6] Perkins, F.W., Phys. Fluids B5 (1993) 477.

[7] Cordey, J.G., and the ITER H-mode database and modelling working group, Energy Confinement scaling and the extrapolation to ITER, 24th EPS Conference on Controlled Fusion and Plasma Physics, Berchtesgaden 1997. Plasma Physics and Controlled Fusion **39** (12B) (1997) B115.

[8] Schissel, D.P., Osborne, T.H., et. al., Vol I, 235, 19th EPS Conference on Controlled Fusionand Plasma Physics, Innsbruck 1992.

[9] Petty, C.C, Luce, T., Nucl. Fusion 37 (1997) 1.

[10] Waltz, R.E., DeBoo, J.C., Rosenbluth, M.N., Phys. Rev. Lett. 65 (199)0 2390.

[11] Waltz, R.E., et al., Nucl. Fusion 32 (1992) 1051.

[12] Christiansen, J.P., Stubberfield, P.M., et. al., Nucl. Fusion 33 (1993) 863.

[13] Petty, C.C., Luce, T., Burrell, K.H., et. al., Phys. Plasmas 2 (1995) 2342.

[14] Cordey, J.G., and the JET Team, IAEA-CN-64/API-1, 16th IAEA Conference on Cont. Fusion Res., Montreal 1996.

[15] Petty, C.C., et. al., P3.038, 24th EPS Conference on Controlled Fusion and Plasma Phys. Berchtesgaden 1997.

[16] Riedel, K.S., Kaye, S.M., Nucl. Fusion 30 (1990) 731.

[17] Lackner, K., Gottardi, N., Nucl. Fusion 30 (1990) 767.

[18] Bateman, G., Phys. Fluids B4 (1992) 634.

[19] Weiland, J., Jarmen, A., Nordman, H., Nucl. Fusion 29 (1989) 1810.
Kotschenreuther, M., Dorland, W., Beer, M.A., Hammett, G.W., Phys. Plasmas 2 (1995) 2381.

[20] Gill, R., et al., Particle and Energy Flow following giant ELMs in JET, IAEA Technical Meeting on H-mode physics, Kloester Seon, Germany, September 1997.

[21] Takizuka, T., Offset Log-Linear Law Scaling for ELMy H-mode Confinement, ITER confinement and Transport workshop, San Diego, April 1997.